

What is the fate of runaway positrons in tokamaks?

Jian Liu,¹ Hong Qin,^{1,2,*} Nathaniel J. Fisch,² Qian Teng,² and Xiaogang Wang³

¹Department of Modern Physics and Collaborative Innovation

Center for Advanced Fusion Energy and Plasma Sciences,

University of Science and Technology of China, Hefei, Anhui 230026, China

²Princeton Plasma Physics Laboratory,

Princeton University, Princeton, NJ 08543

³School of Physics, Peking University, Beijing, China 100871

Abstract

Massive runaway positrons are generated by runaway electrons in tokamaks. The fate of these positrons encodes valuable information about the runaway dynamics. The phase space dynamics of a runaway positron is investigated using a Lagrangian that incorporates the tokamak geometry, loop voltage, radiation and collisional effects. It is found numerically that runaway positrons will drift out of the plasma to annihilate on the first wall, with an in-plasma annihilation possibility less than 0.1%. The dynamics of runaway positrons provides signatures that can be observed as diagnostic tools.

*Electronic address: hongqin@ustc.edu.cn

Positron, the anti-particle of electron, is a rare species in the part of universe where we reside. Since last century, man-made positrons have been generated in accelerators for scientific research, in nuclear reactors as the byproducts, and applied in different fields, such as medicine and material detection [1–3]. Recent researches indicate that tokamak, a magnetic confinement fusion energy device, may be the largest artificial positron factory in the world [4, 5]. In large tokamaks like JET and JT-60U, above 10^{14} positrons are generated in a post-disruption plasma by runaway electrons [6–22]. The dynamics of these positrons after birth in tokamaks is a noteworthy question that may yield valuable information about the runaway dynamics and disruption process in tokamaks. What is the fate of these positrons? Will they annihilate inside the plasma or on the first wall of the vacuum chamber? Because the annihilation probability depends on the path and velocity, the fate of runaway positrons is determined by their phase space trajectories, which are strongly affected by the loop electric field, the helical magnetic field, and the collisional and radiation effects. Incorporating all these factors, we study the phase space dynamics of runaway positrons in tokamaks and predict their final fate.

When relativistic runaway electrons interact with the thermal electrons and ions, positrons are produced in the pair production process. In tokamaks, because the energy of runaway electrons is typically above 10 MeV, most of their “children” positrons are born relativistic and can be accelerated to runaway velocity by the loop voltage. In the toroidal direction, the runaway positrons are accelerated along the toroidal electric field and slowed down by radiation loss and collisions. As the energy increases, strong synchrotron radiation and bremsstrahlung radiation begin to dominate in the drag force, which finally balances the loop electric field force. The collisional drag from the background plasma becomes small after runaway positrons gain high velocities. Nevertheless, the collisional effect offers a momentum transfer mechanism between the parallel and the perpendicular momentum through the pitch-angle scattering. On the other hand, the projection of the positron gyrocenter trajectory onto the poloidal plane is not exactly located on a flux surface due to the geometric effect of the tokamak magnetic field. Numerical results reveal that the circular orbits of runaway positrons in the poloidal plane drift toward or against the major radius direction \hat{e}_R (see Fig.1), under the influence of the loop electric field along the toroidal direction \hat{e}_ϕ and the helical background magnetic field. Due to the drift effect, the runaway positrons hit the first wall of the tokamak within about one hundred milliseconds with energy as large as

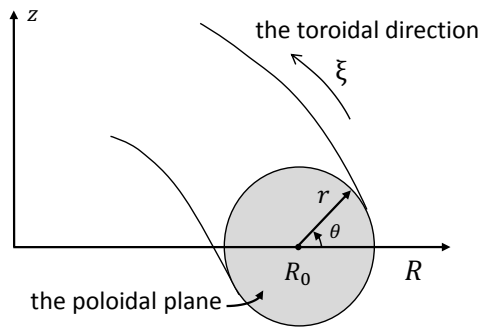


Figure 1: The circular concentric magnetic flux surfaces and the coordinate systems.

150 MeV. After the phase space trajectories are known, the annihilation probabilities along the trajectories can be calculated. For a typical positron, it is found that the probability of annihilation inside the plasma is only about 0.1%. Essentially all positrons generated in the tokamak will annihilate on the first wall of the vacuum chamber. This fact suggests that the annihilation spectrum from the wall can be analyzed to infer the dynamics and distribution of the runaway positions. Admittedly, there are many other loss mechanisms for the positrons. For example, stochastic field lines [23, 24] induced by MHD modes and ripple field [25] can result in transport or orbit loss for energetic positrons. The orbit loss considered in the present study is a neoclassical effect due to the toroidal geometry, and is probably the slowest loss mechanism among all possible mechanisms. The in-plasma annihilation probability of 0.1% obtained in our calculation is thus its upper bound.

We now present in detail the study of phase space dynamics of runaway positrons. For theoretical analysis and numerical simulation, the gyrocenter of runaway positrons is described by a Lagrangian, which incorporates the tokamak geometry, loop voltage, radiation and collisional effects. Parallel momentum, perpendicular momentum, annihilation rate, and the drift orbit in the poloidal plane are numerically calculated as functions of time. The potential of runaway positrons as a diagnostic tool is discussed at the end.

As the anti-particle, the positron has the same rest mass as the electron, denoted as m_e , but opposite electric charge, denoted as e . So the dynamics of runaway positrons are similar to that of runaway electrons. The Lorentz factor for a positron with momentum p is

$$\gamma = \sqrt{1 + \frac{p^2}{m_e^2 c^2}} = \sqrt{1 + \frac{p_{\parallel}^2}{m_e^2 c^2} + \frac{p_{\perp}^2}{m_e^2 c^2}}, \quad (1)$$

where c is the light speed in vacuum, p_{\parallel} is the momentum component parallel to the background magnetic field, and p_{\perp} is the perpendicular momentum. Its synchrotron radiation drag force takes the form

$$F_s = \frac{2}{3} r_e m_e c^2 \gamma (\gamma^2 - 1)^{3/2} \left(\frac{1}{R_0^2} + \frac{\sin^4 \theta}{r_g^2} \right), \quad (2)$$

where $r_e = e^2/4\pi\epsilon_0 m_e c^2$ is the classical positron radius, $r_g = p_{\perp}/eB$ is the positron gyro-radius, θ is the pitch angle defined by $\sin \theta = p_{\perp}/p$, and R_0 is the major radius of the tokamak. The bremsstrahlung drag force is

$$F_B = \frac{4}{137} n_e m_e \gamma c^2 r_e^2 (Z_{eff} + 1) \left(\ln 2\gamma - \frac{1}{3} \right), \quad (3)$$

where n_e is the number density of the background plasma, Z_{eff} is the effective ion charge factor. The collisional friction force is

$$F_c = \frac{n_e e^4 m_e \ln \Lambda \gamma^2}{4\pi\epsilon_0^2 p^2}, \quad (4)$$

where $\ln \Lambda$ is the Coulomb logarithm, which varies slowly with the plasma parameters. To theoretically investigate the dynamics of runaway positrons in tokamaks, we describe the dynamics of positrons by the following Lagrangian [26],

$$L = (e\mathbf{A}_0 + e\mathbf{A}_l + e\mathbf{A}_{eff\parallel} + p_{\parallel}\mathbf{b}) \cdot \dot{\mathbf{x}} - \gamma m c^2. \quad (5)$$

Here, \mathbf{A}_0 is the vector potential of the background magnetic field satisfying $\mathbf{B} = \nabla \times \mathbf{A}_0$, \mathbf{A}_l is the vector potential of the loop electric field satisfying

$$-\frac{\partial \mathbf{A}_l}{\partial t} = \mathbf{E}_{loop}, \quad (6)$$

$\mathbf{A}_{eff\parallel}$ is the parallel component of the effective vector potential corresponding to the drag force,

$$\mathbf{A}_{eff\parallel} = \frac{p_{\parallel}}{p} \frac{t}{e} \left(F_s + F_B + \frac{Z_{eff} + \gamma + 1}{\gamma} F_c \right) \mathbf{b}, \quad (7)$$

and \mathbf{b} is the unit vector along the magnetic field. The magnitude of the effective vector potential in the perpendicular direction is

$$A_{eff\perp} = \frac{p_{\perp}}{p} \frac{t}{e} \left[F_s + F_B + \left(1 - \frac{p_{\parallel}^2}{p_{\perp}^2} \frac{Z_{eff} + 1}{\gamma} \right) F_c \right]. \quad (8)$$

Without loss of generality, we consider a tokamak magnetic field with circular concentric flux surfaces,

$$\mathbf{B} = \frac{B_0 R_0}{R} \hat{\mathbf{e}}_\xi + \frac{B_0 r}{qR} \hat{\mathbf{e}}_\theta. \quad (9)$$

Accordingly we choose its vector potential to be

$$\mathbf{A}_0 = \frac{B_0 R_0 z}{2R} \hat{\mathbf{e}}_R + \frac{B_0 r^2}{2Rq} \hat{\mathbf{e}}_\xi + \frac{R_0 B_0}{2} \ln\left(\frac{R}{R_0}\right) \hat{\mathbf{e}}_z. \quad (10)$$

The loop voltage is set to be

$$\mathbf{E}_{loop} = E_l \frac{R_0}{R} \hat{\mathbf{e}}_\xi. \quad (11)$$

In the right-handed coordinate system (R, ξ, z) (see Fig.1), the Lagrangian takes the form

$$L = p_R \dot{R} + p_\xi \dot{\xi} + p_z \dot{z} - \gamma m_e c^2, \quad (12)$$

where

$$p_R = \frac{e B_0 R_0 z}{2R} - \frac{B_0 z}{B q R} (p_\parallel + e A_{eff\parallel}), \quad (13)$$

$$p_\xi = \frac{e B_0 r^2}{2q} + e A_l R_0 + \frac{B_0 R_0}{B} (p_\parallel + e A_{eff\parallel}), \quad (14)$$

$$p_z = -\frac{e R_0 B_0}{2} \ln\left(\frac{R}{R_0}\right) + \frac{B_0 z}{B q R} (p_\parallel + e A_{eff\parallel}). \quad (15)$$

Because of the toroidal symmetry, i.e. $\partial L / \partial \xi = 0$, the effective toroidal momentum is conserved, i.e.,

$$p_\xi = \frac{\partial L}{\partial \dot{\xi}} = \text{const}. \quad (16)$$

This invariance determines the evolution of p_\parallel as

$$p_\parallel = \frac{B}{B_0 R_0} \left(p_\xi - \frac{e B_0 r^2}{2q} - e A_l R_0 \right) - e A_{eff\parallel}. \quad (17)$$

Meanwhile, there exists another conserved quantity, the effective magnetic moment μ , defined by

$$\mu = \frac{(p_\perp + A_{eff\perp})^2}{2m_e B}, \quad (18)$$

which determines the evolution of p_\perp . If neglecting the higher-order terms caused by the toroidal effect and the poloidal field, Eqs.(17) and (18) give

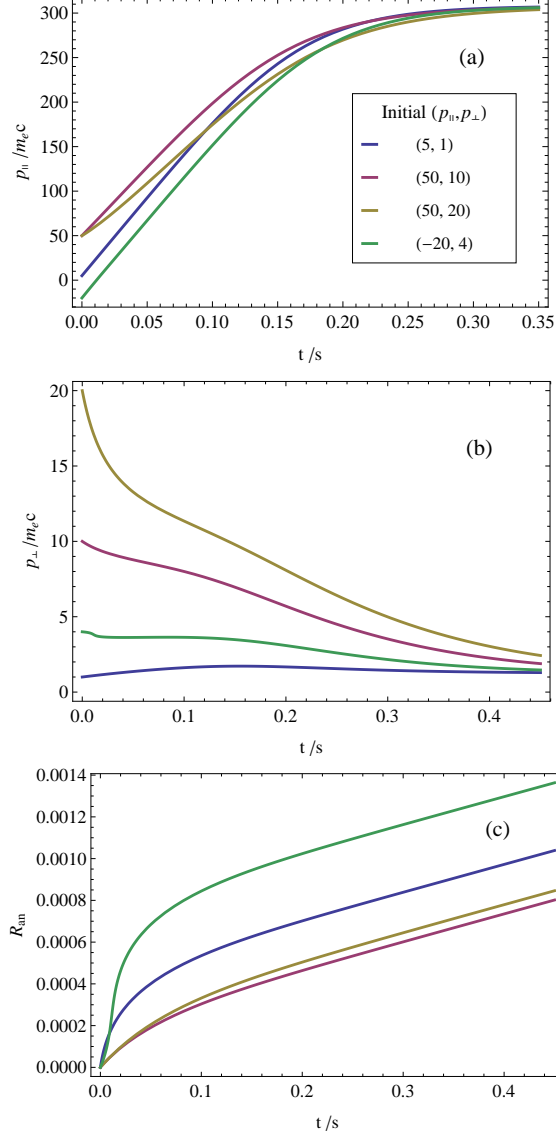


Figure 2: The evolution of the parallel momentum (a), the perpendicular momentum (b), and the annihilation rate (c) of runaway positrons in tokamaks with different initial values of $(p_{\parallel}, p_{\perp})$ (normalized by $m_e c$). The loop electric field is $E_l = 3V/m$.

$$\frac{dp_{\parallel}}{dt} = eE_{loop} - \frac{p_{\parallel}}{p} \left(F_s + F_B + \frac{Z_{eff} + \gamma + 1}{\gamma} F_c \right),$$

$$\frac{dp_{\perp}}{dt} = -\frac{p_{\perp}}{p} \left[F_s + F_B + \left(1 - \frac{p_{\parallel}^2}{p_{\perp}^2} \frac{Z_{eff} + 1}{\gamma} \right) F_c \right],$$

which are consistent with the momentum evolution equations in [12, 27–29]. After substituting Eqs.(17) and (18) into Eq.(12) and dropping the term $p_{\xi} \dot{\xi}$, the toroidal symmetry

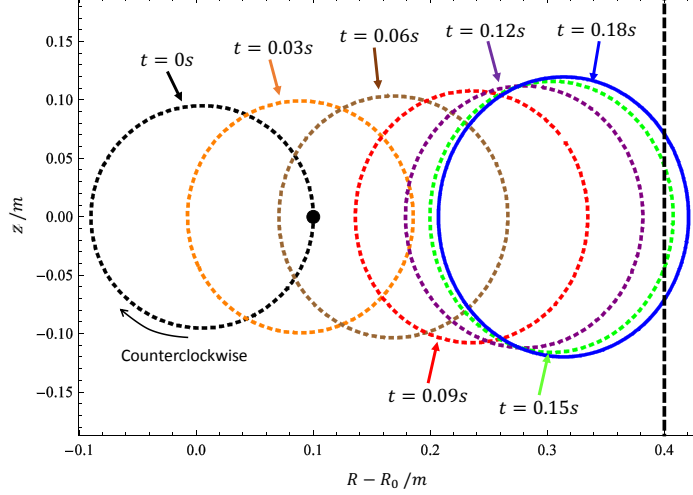


Figure 3: Snapshots, taken for every $0.03s$, of the circular orbit of a runaway positron in the poloidal plane, with initial position $R - R_0 = 0.1m$, $z = 0m$ and initial momenta $p_{\parallel} = 5m_e c$ and $p_{\perp} = m_e c$. The loop electric field is $E_l = 5V/m$. The position of the first wall is indicated by the dashed vertical line.

leads to the reduced Lagrangian in the (R, z) 2D space

$$L = p_R(R, z)\dot{R} + p_z(R, z)\dot{z} - H(R, z). \quad (19)$$

This is the procedure of Routh reduction. Then the runaway positron dynamics in the 2D configuration space, i.e., the projection poloidal plane, is given by the Euler-Lagrangian equation,

$$\dot{R} = \frac{\partial H / \partial z}{\partial p_R / \partial z - \partial p_z / \partial R}, \quad (20)$$

$$\dot{z} = \frac{\partial H / \partial R}{\partial p_z / \partial R - \partial p_R / \partial z}. \quad (21)$$

Equations (17), (18), (20) and (21) determines the dynamics of runaway positrons in phase space. Given the dynamics in the momentum space, the in-plasma annihilation probability of a runaway positron can be calculated according to

$$R_{an} = \int_0^t n_e \sigma_{an} v d\tau, \quad (22)$$

where the annihilation cross-section for the positron-electron reaction is [5]

$$\sigma_{an} = \frac{\pi r_e^2}{1 + \gamma} \left[\frac{\gamma^2 + 4\gamma + 1}{\gamma^2 - 1} \ln(\gamma + \sqrt{\gamma^2 - 1}) - \frac{\gamma + 3}{\sqrt{\gamma^2 - 1}} \right] \frac{2\pi}{137p(1 - e^{-2\pi/137p})}. \quad (23)$$

To guarantee the long term numerical accuracy and fidelity, we have adopted a variational symplectic integrator [30, 31], which discretizes the Lagrangian directly, to carry out the numerical simulation. For conventional integration algorithms, such the Runge-Kutta method, numerical errors from different time-steps accumulate coherently and the error grows without bound for long-term simulations. In comparison, the variational symplectic integrator can globally bound the numerical error for all time-steps, and thus are superior for simulating the runaway dynamics, which often involves many hundreds of thousands of turns in the poloidal plane.

For the present study, we use the parameters from EAST as a specific example [32]. We set $B_0 = 3.5T$, $R_0 = 1.7m$, $n_e = 10^{19}m^{-3}$, and $\ln \Lambda = 10$. The loop electrical field is $E_l = 3V/m$, and the minor radius is $a = 0.4m$. In typical EAST operations, the safety factor q varies in the range of 1 to 3, while the profile of q is rather flat in the core region. Thus we choose $q = 2$ in the calculation. For runaway positrons with different initial parallel and perpendicular momentum, their momentum evolution are plotted in Fig.2. After 0.3s, all the parallel momenta reach a steady value around $300m_e c$, as a result of the balance between the loop electric field acceleration and the drag force resistance. The perpendicular momenta also evolve towards a steady value, though a little slower, due to the balance between the radiation loss and the momentum transfer from parallel direction through the pitch angle scattering. The green curves show the dynamics of what might be called a "backward runaway" positron [33, 34], whose initial parallel momentum is opposite to the loop electric field. It undergoes a deceleration under in the toroidal direction at first. However, its parallel momentum reverses sign after 0.01s and then increases like forward runaway positrons with positive parallel momenta. Its perpendicular momentum has a drop in the deceleration phase and passes a point of inflexion at 0.01s. It can be seen that runaway positrons of widely different initial momentum nonetheless approach attractor curves in momentum space. The existence of attractor curves is made possible because of the dissipation introduced by radiation effects.

The possibility of annihilation for runaway positrons with different initial momenta is depicted in Fig.2(c). Because the annihilation cross-section becomes very large when the positron moves slowly relative to the background electrons, the annihilation rate of the

positron with negative parallel momentum grows rapidly during its turning around process. Nevertheless, it escaped from the doom of annihilation for a non-relativistic positron. Though its parallel momentum goes through zero, its perpendicular momentum is still relativistic, which ensures that it is not annihilated in the slowing-down process and can be accelerated to runaway in the backward direction. Overall, the annihilation probability is very low for runaway positrons. The probability is only about 0.1% after 0.4s, which is long enough for runaway positrons to escape the tokamak plasmas through the drift motion or other transport/loss mechanisms in the poloidal plane.

The motion of a runaway positron in the poloidal plane with loop electric field $E_l = 5V/m$ is depicted in Fig.3. The loop electric field and the toroidal magnetic field are in the \hat{e}_ξ direction, and the poloidal magnetic field is in the \hat{e}_θ direction. The counterclockwise circular orbits are snapshotted for every 0.03s. The outward drift of the circular orbit to the \hat{e}_R direction is evident. The drift velocity slows down with the radiation resistance in the toroidal direction increases. The drift velocity can be roughly estimated as $v_{dr} = q(E_l + E_{eff\parallel})/B_0$ [13]. The runaway positron finally hits the wall before $t = 0.15s$, with an in-plasma annihilation probability less than 0.1%. This example illustrates the fact that most of the runaway positrons in tokamaks can drift out of the plasma to hit the wall before annihilation within the plasma. If the safety factor $q = q(R, z)$ is a function of the spatial coordinates like in real tokamaks, the drift velocity will explicitly depend on the spatial location. However, the space-dependent safety factor also leads to similar runaway positron dynamics and the same main conclusions as the constant- q assumption. For situations with larger loop electric field, the runaway positrons will drift faster. If changing the helical direction of the magnetic field or the direction of the loop electric field, the positron will drift inwards, i.e., towards the negative \hat{e}_R direction, to hit the inner wall. It is observed that the radius of circular orbit varies as the positron drifts along the \hat{e}_R direction, especially in the later stage. As mentioned previously, the neoclassical orbit loss is just one of many loss mechanisms for positrons. Since other loss mechanisms [23–25, 28, 35–37] are in general faster, the in-plasma annihilation probability observed in experiments should be even less. Finally, because the orbit drift does not depend on the electric charge, note that runaway electrons, which will have their own signature (like visible damage to the wall), will strike exactly on the same side of the vacuum vessel.

Early in 1986, Surko et al. proposed to diagnose the transport process by injecting

positrons into tokamaks [38]. The annihilation spectrum of positrons in thermal plasmas was also studied [39]. Now it is clear that the large amounts of positrons produced by tokamaks themselves can be used as a diagnostic tool as well. Since most of the positrons are annihilated outside the plasma, the positron diagnostic in tokamaks cannot detect plasma properties directly as in PET (Positron Emission Tomography) [1]. However, positron diagnostic is still possible using our knowledge of the dynamics of the runaway positrons. The annihilation spectrum, which can be recorded by the gamma spectrometer, is very characteristic and easily identifiable. The intensity, breadth, and shift of the annihilation peak in the spectrum reflect the properties of the plasma that determines the runaway dynamics. Moreover, the time history of the positron annihilation is also an important indication to some events in tokamaks, such as a disruption or rf heating, which produce a burst of positron runaways at a specific time. The annihilation locations on the first wall and the emission directions of the gamma ray provide information about the phase space coordinates of the runaway positrons at the end of their journey, from which we can also infer the trajectories of runaway electrons in the phase space. Theoretical and experimental studies on these topics will be reported in future publications.

Acknowledgments

This research is supported by the JSPS-NRF-NSFC A3 Foresight Program in the field of Plasma Physics (NSFC-11261140328), the National Natural Science Foundation of China (NSFC-11305171), ITER-China Program (2014GB124005 and 2013GB111000), the Fundamental Research Funds for the Central Universities (WK2030020022), and the CAS Program for Interdisciplinary Collaboration Team. We thank Professor Tieshuan Fan and Di Hu for fruitful discussion.

-
- [1] D. L. Bailey, D. W. Townsend, P. E. Valk, and M. N. Maisey, *Positron Emission Tomography: Basic Sciences* (2005).
 - [2] R. Siegel, *Annu. Rev. Mater. Sci.* **10**, 393 (1980).
 - [3] A. Van Veen, F. Labohm, H. Schut, J. De Roode, T. Heijenga, and P. Mijnders, *Appl. Surf. Sci.* **116**, 39 (1997).

- [4] P. Helander and D. J. Ward, Phys. Rev. Lett. **90**, 135004 (2003).
- [5] T. Fülöp and G. Papp, Phys. Rev. Lett. **108**, 225003 (2012).
- [6] H. Dreicer, Phys. Rev. **115**, 238 (1959).
- [7] R. M. Kulsrud, Y.-C. Sun, N. K. Winsor, and H. A. Fallon, Phys. Rev. Lett. **31**, 690 (1973).
- [8] J. Connor and R. Hastie, Nucl. Fusion **15**, 415 (1975).
- [9] P. Helander, L. Eriksson, and F. Andersson, Plasma Phys. Control. Fusion **44**, B247 (2002).
- [10] H. Knoepfel and D. A. Spong, Nucl. Fusion **19**, 785 (1997).
- [11] M. N. Rosenbluth and S. V. Putvinski, Nucl. Fusion **37**, 1355 (1997).
- [12] M. Bakhtiari, G. Kramer, and D. G. Whyte, Phys. Plasmas **12**, 102503 (2005).
- [13] X. Guan, H. Qin, and N. J. Fisch, Phys. Plasmas **17**, 092502 (2010).
- [14] R. D. Gill, B. Alper, A. W. Edwards, L. C. Ingesson, M. F. Johnson, and D. Ward, Nucl. Fusion **40**, 163 (2000).
- [15] R. D. Gill, Nucl. Fusion **33**, 1613 (1993).
- [16] R. Jaspers, N. J. L. Cardozo, A. J. H. Donné, H. L. M. Widdershoven, and K. H. Finken, Rev. Sci. Instrum. **72**, 466 (2001).
- [17] R. Jaspers, K. Finken, G. Mank, F. Hoenen, J. Boedo, N. Cardozo, and F. Schuller, Rev. Sci. Instrum. **33**, 1775 (1993).
- [18] J. M. Adamsb, O. N. Jarvis, G. J. Sadlera, D. B. Symea, and N. Watkinsb, Nucl. Instrum. Methods A **329**, 277 (1993).
- [19] H. Bolt, A. Miyahara, M. Miyake, and T. Yamamoto, J. Nucl. Mater. **151**, 48 (1987).
- [20] R. Nygren, T. Lutz, D. Walsh, G. Martin, M. Chatelier, T. Loarer, and D. Guilhem, J. Nucl. Mater. **241**, 522 (1997).
- [21] H.-W. Bartels, Fusion Eng. Des. **23**, 323 (1994).
- [22] T. Kawamura, H. Obayashi, and A. Miyahara, Fusion Eng. Des. **9**, 39 (1989).
- [23] R. Yoshino and S. Tokuda, Nucl. Fusion **40**, 1293 (2000).
- [24] P. Helander, L.-G. Eriksson, and F. Andersson, Phys. Plasmas **7**, 4106 (2000).
- [25] J. M. Rax, N. J. Fisch, and L. Laurent, Plasma Phys. Control. Fusion **35**, B129 (1993).
- [26] C. Grebogi and R. G. Littlejohn, Phys. Fluids **27**, 1996 (1984).
- [27] J. R. Martín-Solís, J. D. Alvarez, R. Sánchez, and B. Esposito, Phys. Plasmas **5**, 2370 (1998).
- [28] J. R. Martín-Solís, B. Esposito, R. Sánchez, and J. Alvarez, Phys. Plasmas **6**, 238 (1999).
- [29] F. Andersson, P. Helander, and L.-G. Eriksson, Phys. Plasmas **8**, 5221 (2001).

- [30] H. Qin and X. Guan, *Phys. Rev. Lett.* **100**, 035006 (2008).
- [31] H. Qin, X. Guan, and W. M. Tang, *Phys. Plasmas* **16**, 042510 (2009).
- [32] S. Wu, *Fusion Eng. Des.* **82**, 463 (2007).
- [33] C. F. F. Karney and N. J. Fisch, *Phys. Fluids* **29**, 180 (1986).
- [34] N. J. Fisch, *Rev. Mod. Phys.* **59**, 175 (1987).
- [35] M. Lehnen, S. A. Bozhenkov, S. S. Abdullaev, TEXTORTeam, and M. W. Jakubowski, *Phys. Rev. Lett.* **100**, 255003 (2008).
- [36] G. Papp, M. Drevlak, T. Fülöp, P. Helander, and G. Pokol, *Plasma Phys. Control. Fusion* **53**, 095004 (2011).
- [37] K. Finken, S. Abdullaev, M. Jakubowski, R. Jaspers, M. Lehnen, R. Schlickeiser, K. Spatschek, A. Wingen, R. Wolf, et al., *Nucl. Fusion* **47**, 91 (2007).
- [38] C. Surko, M. Leventhal, W. Crane, A. Passner, F. Wysocki, T. Murphy, J. Strachan, and W. Rowan, *Rev. Sci. Instrum.* **57**, 1862 (1986).
- [39] U. O. Ziemelis, Ph.D. thesis, The University of British Columbia (1976).